Magnetic Properties of Polycrystalline $PrCu_2$: A Quadrupolar Transition Material

Jesús Rodríguez Fernández

CITIMAC, Facultad de Ciencias, Universidad de Cantabria, 39005 Santander, Spain

Reprint requests to Prof. J. Rodríguez Fernández. Fax: +34 942 201402. E-mail: rodrigufj@unican.es

Z. Naturforsch. **2007**, *62b,* 941 – 948; received April 3, 2007

Dedicated to Dr. Bernard Chevalier on the occasion of his 60th birthday

Polycrystalline $PrCu_2$, which has a quadrupolar transition at 7.7 K, has been investigated using electrical resistivity, magnetization and dilatometry techniques. To study dilution effects, two solid solutions of $PrCu_2$, $(Pr_{0.8}La_{0.2})Cu_2$, and $(Pr_{0.8}Y_{0.2})Cu_2$, were also studied. The quadrupolar transition decreases in temperature with doping, while it increases slightly with the magnetic field. In resistivity and thermal expansion, the magnetic contributions show a clear evidence of crystal field excitations. The analysis of both properties provided benchmark values of the Debye temperature and Grüneisen parameters.

Key words: Quadrupolar Effects, $PrCu_2$, Magnetic Properties, Electrical Resistivity, Crystal Field

Introduction

When ions with localized electrons such as in $4f$ or $5f$ shells have a nonmagnetic ground state, *i. e.* no dipolar moment in the ground state, the ions usually remain paramagnetic down to very low temperatures where ordering of nuclear moments might occur and induce electronic moments as in Pr. However, as recently pointed out [1], the ions can also undergo another type of transition induced by asymmetric charge distribution of f electrons, a so called quadrupolar transition. The nature of this quadrupolar transition is very interesting and not yet fully understood. Until now, quadrupolar transitions have been extensively studied in systems with cubic symmetry. However, this transition was also recently found to exist in compounds such as UPd_3 [2] and $PrCu_2$ [3, 4] with different symmetry.

$PrCu_2$ crystallizes in the orthorhombic KHg_2-type which can be regarded as a distorted hexagonal AlB_2 structure where the orthorhombic b axis is the hexagonal c axis of the AlB_2 structure. The C_{2v} local symmetry at the Pr site of $PrCu_2$ splits the ninefold degenerate multiplet $^3H_4$ of the Pr^{3+} ion into nine singlets. Although the ground state is expected to be non-magnetic, it has a non-zero quadrupolar moment. It appears that the energy separation between the two lowest singlets decreases below 8 K, and Pr undergoes a quadrupolar transition. When Pr enters the quadrupolar ordered phase, quadrupole moments are coupled to each other through lattice strains leading to a crystal symmetry transformation from orthorhombic to monoclinic [5]. With lowering the temperature further, the material becomes antiferromagnetically ordered at 54 mK, which involves both the conduction electron and the nuclear spins [6 – 8]. Recently, muon spin rotation spectroscopy has demonstrated that this magnetic order continues to be present, at least on a short-range scale, up to at least 60 K, the quadrupolar-quadrupolar coupling being the proposed driving mechanism [9].

Naturally, crystal field excitations of $PrCu_2$ have been a central issue regarding the quadrupolar transition and were studied intensively using different techniques. Early specific heat measurements [10] indicated that the separation between the first two levels is $\Delta_1 \ll 7$ K at $T \geq 8$ K and $\Delta_1 \sim 15$ K at 0 K. On the other hand, inelastic neutron studies [11] gave a more accurate estimate for the first four levels; separations between the ground state and the three excited states are $\Delta_1 = 6$ K, $\Delta_2 \sim 6$ K and $\Delta_3 = 15$ K. These values change slightly below 8 K to $\Delta_1 = 3$ K, $\Delta_2 = 12$ K and $\Delta_3 = 15$ K.

Using susceptibility and magnetization results, two groups [12, 13] independently proposed similar level schemes with total crystal field splittings of 316

Compound	a (Å)	b (Å)	c (Å)	V (Å^3)	R_{Bragg}
$PrCu_2$	4.411(3)	7.058(4)	7.448(4)	231.9(5)	0.13
$(Pr_{0.8}La_{0.2})Cu_2$	4.420(4)	7.117(5)	7.471(6)	235.0(6)	0.17
$(Pr_{0.8}Y_{0.2})Cu_2$	4.387(4)	7.022(6)	7.411(5)	228.3(6)	0.19
YCu_2	4.305(3)	6.876(5)	7.296(5)	216.0(5)	0.15

Table 1. Cell parameters and volume of the compounds.

and 230 K. However, in both cases, the lowest energy levels do not compare well with the inelastic neutron results. Incorporating the inelastic neutron results with susceptibility data, another level scheme was proposed by Ahmet *et al.* [3] with a total splitting energy nearly twice that given in refs. [12] and [13].

High-field magnetization and deHaas-van Alphen (dHvA) experiments have shown that $PrCu_2$ has a new type of metamagnetic transition along the c axis [14, 15]. According to these results, a magnetic hard axis (c axis) becomes an easy axis (a axis), and *vice versa*, above the metamagnetic transition. The conversion of easy and hard axes has been reported only for $DyCu_2$ [16] of the same orthorhombic $PrCu_2$ structure. The physical origin of the axis conversion has been interpreted in terms of the rotation of quadrupolar moments on the *ac* plane, which appears to be easier due to the similarity between the orthorhombic and the hexagonal AlB_2-type structure of $PrCu_2$ as mentioned before.

Regarding our present contribution to the study of this material, it is worth mentioning that there have been relatively few reports on the macroscopic properties of polycrystalline $PrCu_2$ between r. t. to lower temperatures. It is the aim of this communication to report susceptibility, thermal expansion and resistivity data of $PrCu_2$ between 2 and 300 K and to discuss the crystal field effects seen in these macroscopic measurements. The effects of Pr dilution have been studied as well. Because $LaCu_2$ has a different crystal structure, we used YCu_2 with the same KHg_2-type structure as our non-magnetic material.

Experimental Details

Stoichiometric amounts of Pr (99.99 %), Y (99.99 %) and Cu (99.99 %) were melted using an induction furnace under high vacuum. We subsequently made X-ray powder diffraction measurements (XRD) of all the samples using Bragg-Brentano geometry and CuK_α radiation. The electrical resistivity was measured on parallelepiped samples using a standard ac four-point technique [17] between 2 K and r. t. For magnetic measurements, we used a SQUID magnetometer (Quantum Design, MPMS7) from 2 K to r. t. and fields up to 7 T. Thermal expansion was measured between 10 and 300 K using a strain gauge technique at Universidad de Cantabria and between 1.8 and 30 K using a capacitance cell at University College, London. High field measurements were made using an extraction magnetometer of the high magnetic field laboratory, Grenoble.

Results and Analysis

X-Ray diffraction studies

XRD patterns of the compounds were measured and then analyzed by means of the Rietveld method using the program FULLPROF [18]. We found that all samples were well crystallized, presenting a single phase (space group *Imma*) with lattice parameters given in Table 1. The lattice parameters of $PrCu_2$ are in agreement with those previously reported. La substitution increases the cell volume whereas Y substitution reduces it, as expected from the different ionic radii: Pr^{3+} (1.013 Å), La^{3+} (1.061 Å) and Y^{3+} (0.88 Å).

Electrical resistivity

A plot of the temperature dependence of the electrical resistivity for all compounds is shown in Fig. 1. Resistivity of $PrCu_2$ has a well defined change of curvature at T_Q = 7.7 K which corresponds to the quadrupolar order transition. Although the resistivity continues

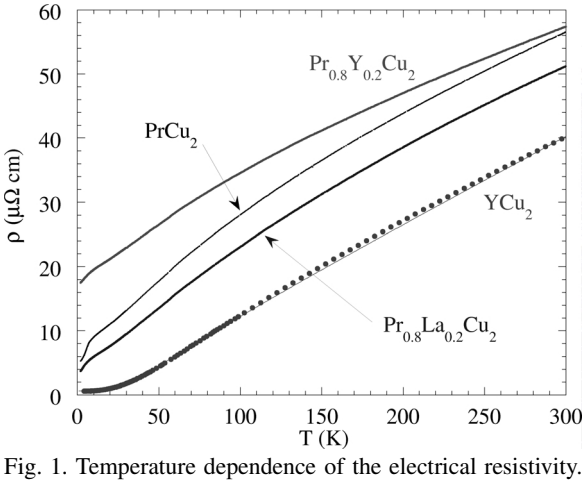

Fig. 1. Temperature dependence of the electrical resistivity. In YCu_2, dots represent experimental points and the straight line the fitting to the Grüneisen-Bloch law.

Table 2. Electrical resistivity data.

Compound	ρ_{res} ($\mu\Omega$ cm)	dρ/dT ($\mu\Omega$ cm K^{-1}) at 300 K	ρ_{m0} ($\mu\Omega$ cm)
$PrCu_2$	5.1	0.122	13
$(Pr_{0.8}La_{0.2})Cu_2$	3.5	0.122	9.8
$(Pr_{0.8}Y_{0.2})Cu_2$	17.2	0.101	8
YCu_2	0.6	0.128	

to decrease below 2 K, the residual resistivity (ρ_{res}) can be estimated by an extrapolation to $T = 0$ K from the data above 2 K. We recall that residual resistivities usually follow the Nordheim rule with doping [19]. This is the case for the Y-doped sample, which has a ρ_{res} value higher than that observed for pure $PrCu_2$ (see Table 2). However, it is unexpected to have ρ_{res} of $Pr_{0.9}La_{0.2}Cu_2$ lower than that of the pure compound. This feature evidences that in spite of the additional chemical disorder due to La substitution, the total lattice disorder is lower in $Pr_{0.8}La_{0.2}Cu_2$ than in $PrCu_2$ indicating a better crystallization of the 20 % La sample.

Resistivity of YCu_2 shows a typical metallic behaviour due to electron-phonon scattering. It can be fitted using the Grüneisen-Bloch law (full line in Fig. 1) with a Debye temperature Θ_D = 163 K. Allowing for corrections due to the mass difference between Y and Pr, we estimate that the Debye temperatures are 147 K for $PrCu_2$ and 149.4 K for $Pr_{0.9}La_{0.2}Cu_2$. High-temperature slopes $\beta = d\rho/dT$ are almost the same for all three compounds and similar to those found in *RE*Pt (*RE* = rare earth element) compounds, $\beta = 0.125\ \mu\Omega\,\mathrm{cm}^{-1}$ [20], the only exception being the Y-doped one which has a lower value of β.

Using the Θ_D and β values we can first calculate the phonon contributions ρ_{phon} for each compound using the Grüneisen-Bloch law and, subsequently, the magnetic resistivity from the relationship $\rho_m = \rho - \rho_{res} - \rho_{phon}$ (for details see ref. [21]). Fig. 2 shows magnetic resistivities obtained from the procedure just described. In the magnetic resistivity of $PrCu_2$, we observe one clear anomaly arround 7 K corresponding to the quadrupolar transition, followed by a noticeable reduction of ρ upon decreasing T (see the insert in Fig. 2). With doping, this anomaly at low temperature gets subdued considerably, and we do not observe a clear anomaly for the doped sample although the resistivity curvature increases at lower temperatures. From the magnetization data to be discussed below we found that the transition temperature moves towards lower temperatures upon doping. One noteworthy point about the general shape of the resistivity curve for $PrCu_2$ is that it exhibits strong crystal field effects on ρ_m above the quadrupolar transition. The magnetic resistivity shows a large increase in the paramagnetic region due to scatterings from excited crystal field levels. When temperature increases and all the CEF levels are equally populated, ρ_m tends to reach its maximum value ρ_{m0} [22]. Similar behaviour is also observed in the diluted compounds, which show lower values of ρ_{m0} as compared with that of $PrCu_2$ in agreement with the reduction in Pr concentration.

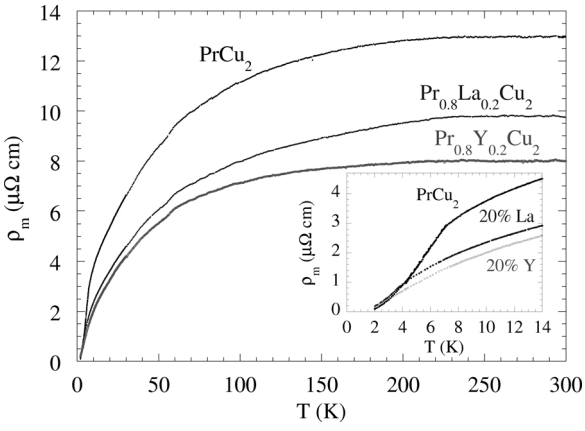

Fig. 2. Temperature dependence of the magnetic resistivities. The insert shows the low temperature part.

To analyze the magnetic resistivity data further, we used a model given by Rao and Wallace [23], according to which the magnetic resistivity can be written in the following form:

$$\rho = \rho_{m0}\frac{2}{J(J+1)}\sum_{m_s,m_{s'},i,i'}|\langle m_s' i'|sJ|m_s i\rangle|^2 p_i f_{ii},$$

where m_s and m_s' are spins of conduction electrons in initial and final states; i and i' are crystal field states with energies E_i and $E_{i'}$. Matrix elements are between *eigenstates* for local moment and conduction electron systems.

$$p_i = \frac{\exp[-E_i/k_B T]}{\sum_j \exp[-E_j/k_B T]}$$

and

$$f_{ii'} = \frac{2}{1+\exp[-(E_i - E_{i'})/k_B T]}$$

Using this formula we calculated the $\rho_m(T)$ contribution for $PrCu_2$. We compare the calculated $\rho_m(T)$ val-

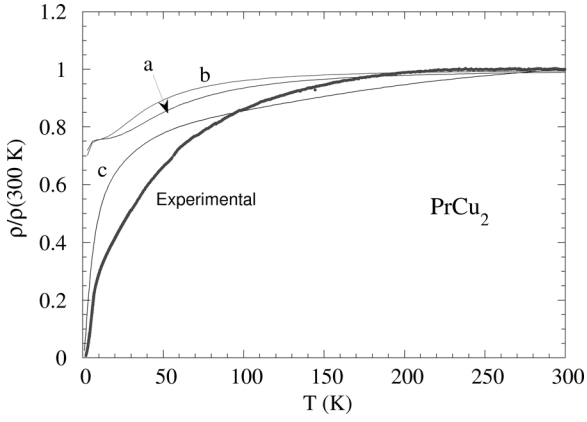

Fig. 3. Comparison between experimental and calculated $\rho_m(T)$. The CEF parameters for the a, b and c curves are taken from references [12, 13] and [3], respectively.

ues with the experimental results in Fig. 3. Lines a and b are for calculated results using crystal field parameters given in refs. [12] and [13], respectively. We also calculated the magnetic resistivity using the CEF parameters from ref. [3] (line c in Fig. 3). Qualitatively the models account for the increase of the resistivity with temperature in the paramagnetic region. However, quantitatively none of the three CEF models can fit properly the experimental data although overall line c is in better agreement with the experimental results. The largest differences between experimental data and the model are found in the low-temperature region, probably associated with the influence of the short range magnetic order observed up to 60 K [9] by muon spin rotation spectroscopy.

Magnetization and susceptibility

Fig. 4 shows the magnetization measured in an applied magnetic field of $B = 0.1$ T. Measurements were made with increasing temperature after cooling the sample to 2 K in zero field. Magnetization of $PrCu_2$ shows a slight upturn at $T = 7.7$ K, corresponding to the quadrupolar transition. In $Pr_{0.9}La_{0.2}Cu_2$ and $Pr_{0.9}Y_{0.2}Cu_2$, there are slight upturns at lower temperatures. This behaviour is clearly revealed in the derivative of the magnetization (insert of Fig. 4), where a negative peak is observed for all three compounds. Thus, quadrupolar transition temperatures for $Pr_{0.9}La_{0.2}Cu_2$ and $Pr_{0.9}Y_{0.2}Cu_2$ are found to be 4.9 and 5.4 K, respectively. It is important to point out that alloying effects in other quadrupolar transition material, such as UPd_3, destroy the quadrupolar order even with percentages lower than 5 % [24].

To study the field dependence of the quadrupolar transition of $PrCu_2$, we measured the temperature dependence of the magnetization up to 7 T. Fig. 5 shows the derivative of the magnetization at several fields. The position of the peak changes very little with fields up to 7 T. Regarding this field dependence of the quadrupolar transition of $PrCu_2$, it is worth mentioning that in TmCd the quadrupolar transition temperature increases appreciably even with a small magnetic field [25].

Although all the proposed crystal field schemes for $PrCu_2$ have an overall energy level splitting larger than 230 K, the temperature dependence of the inverse magnetic suceptibility is almost linear down to 20 K.

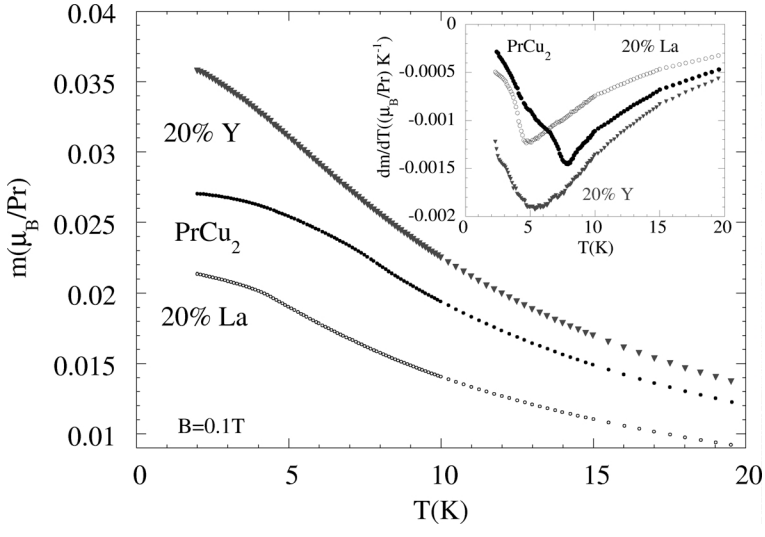

Fig. 4. Magnetic moment per Pr ion in an applied field of 0.1 T. The insert shows the temperature derivative.

Compound	Magnetization per Pr ion (μ_B) at 2 K and 0.1 T	θ_p (K)	μ_{eff} (μ_B)	χ_0 (emu mol^{-1})	T_Q (K)
$PrCu_2$	0.0271	−2.5	3.56	-2.2×10^{-4}	7.9
$(Pr_{0.8}La_{0.2})Cu_2$	0.0214	−10.4	3.50	-6.6×10^{-4}	4.9
$(Pr_{0.8}Y_{0.2})Cu_2$	0.0358	3.7	3.51	-4.8×10^{-4}	5.4

Table 3. Main magnetic parameters.

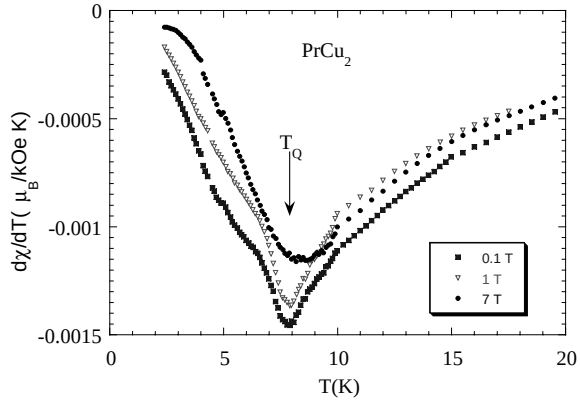

Fig. 5. Temperature derivative of the $PrCu_2$ susceptibility measured at different applied fields.

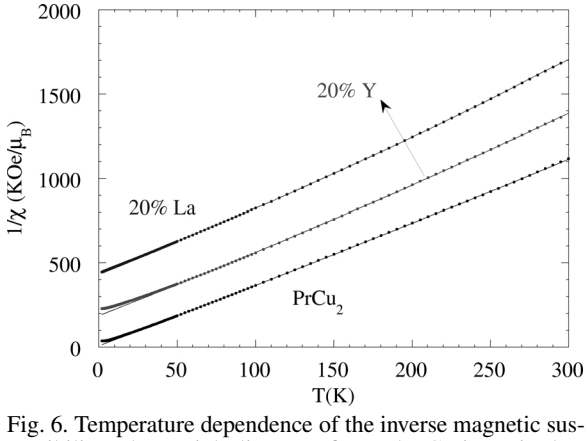

Fig. 6. Temperature dependence of the inverse magnetic susceptibility. The straight lines are fits to the Curie-Weiss law above 20 K. For the sake of clarity, the data for each compound are shifted upwards.

A similar linear dependence has also been observed in the diluted compounds, although these materials show a slightly positive curvature (Fig. 6). The data have been fitted well using a modified Curie-Weiss law $\chi = \chi_0 + C/(\theta - \theta_p)$ between 20 and 300 K (solid lines in Fig. 6). In $PrCu_2$, the best fit produces an effective moment $\mu_{eff} = 3.56\ \mu_B$, $\chi_0 = -2.2\times10^{-4}$ emu/mole and $\theta_p = -2.5$ K. This effective moment value is very close to the theoretical value of the Pr^{3+} ion ($\mu_{eff} = 3.58\ \mu_B$). The Curie-Weiss temperature is negative for $PrCu_2$,

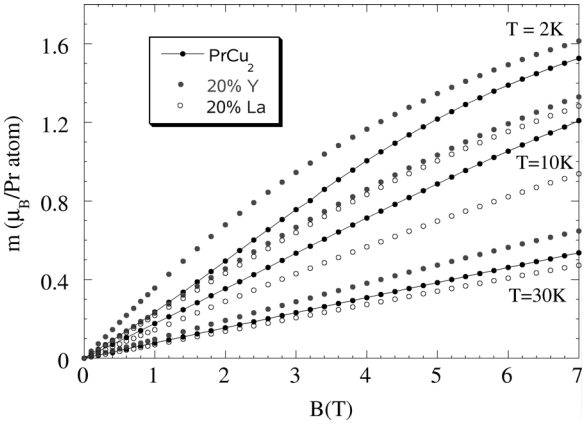

Fig. 7. Magnetic moment *versus* magnetic field at T = 2, 10 and 30 K.

indicative of the presence of weak antiferromagnetic correlations. For the diluted compounds, μ_{eff} is similar but θ_p becomes positive for 20 % Y (see Table 3). Magnetization was also measured up to 7 T at several temperatures (see Fig. 7). In the T = 2 K curves, at temperatures well below the quadrupolar transitions, a small change of curvature is observed in $PrCu_2$ at B = 2 T whereas a clear negative curvature is observed for the dilute compounds.

We also measured the high-field magnetization up to 20 T (see Fig. 8). Two observations are noteworthy in our data. First, the magnetization begins to level off above 7 T and appears to saturate towards the value of 2.2 μ_B per Pr ion. This value is in agreement with the average of the values obtained along the three crystallographic axes in a single crystal [3]. With increasing temperature, this saturation behaviour disappears rapidly. The curves do not show any distinctive anomaly which could be related to the metamagnetic transition observed along the c axis, so this transition is probably suppressed in polycrystalline samples. A second point concerns the magnetization *versus* temperature plot (not shown here). Although we acknowledge that data get somewhat scattered with increasing fields, and it becomes difficult to get dM/dT with reasonable accuracy as previously obtained with the SQUID data below 7 T, it appears that the quadrupolar transi-

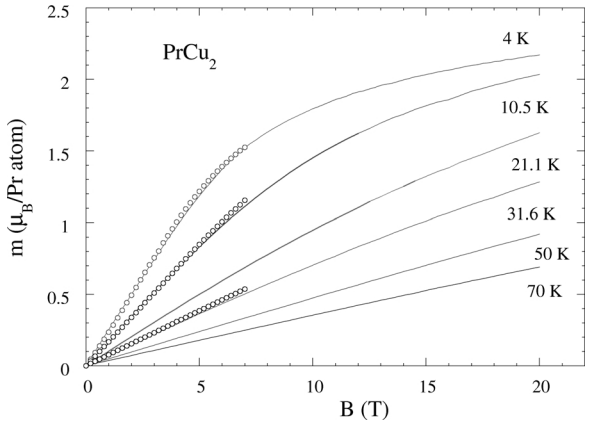

Fig. 8. Magnetization curves of $PrCu_2$ at several temperatures up to 20 T. In circles are shown for comparison some SQUID data up tp 7 T.

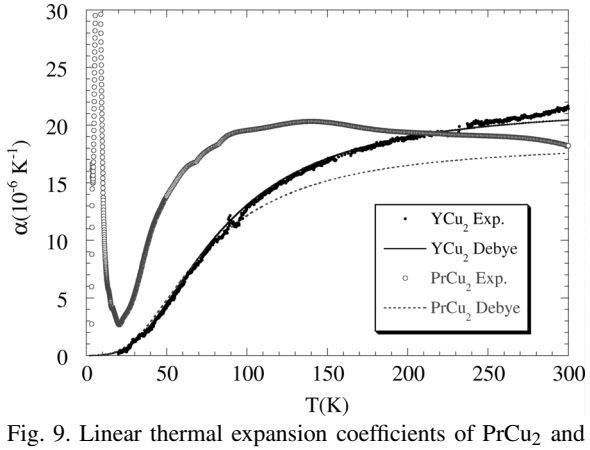

Fig. 9. Linear thermal expansion coefficients of $PrCu_2$ and YCu_2. The solid line represents the Debye fit whereas the dashed line represents the estimated phonon contribution of $PrCu_2$.

tions do not seem to change much with field even up to 20 T.

Thermal expansion

We measured the thermal expansion of the compounds $PrCu_2$ and YCu_2. The relative change of length $\Delta L/L$ between 4 and 300 K is 4200×10^{-6} and 5500×10^{-6} for YCu_2 and $PrCu_2$, respectively. Fig. 9 shows the temperature dependence of the thermal expansion coefficient $\alpha = (1/L)\,(\mathrm{d}L/\mathrm{d}T)$. The curve of the non-magnetic YCu_2 shows a typical behaviour due to phonons. We can fit the YCu_2 data using a relation between thermal expansion and specific heat (C_v) $\alpha = \Gamma\chi C_v/3V_m$, where Γ is the Grüneisen parameter, χ is the compressibility and V_m the molar volume. The best fit (solid line in Fig. 9) is obtained with a Debye temperature Θ_D = 340 K and $\Gamma\chi = \partial \ln \Theta_D/\partial P$ = 2.8 Mbar^{-1}. This Θ_D is larger than that calculated using the resistivity. Differences between Θ_D values obtained using different techniques have previously been reported for other compounds [26]. For example, for YNi and LaNi the Debye temperature obtained from thermal expansion is also higher than that from resistivity [27]. At r. t. the α value is lower for $PrCu_2$ than for YCu_2. This, we think, is due to the smaller value of $\Gamma\chi$ for $PrCu_2$ ($\Gamma\chi$ = 2.6 Mbar^{-1}) than that for YCu_2 ($\Gamma\chi$ = 2.8 Mbar^{-1}). In order to extract the magnetic contributions to the thermal expansion (α_m), we have subtracted the phonon contribution $\alpha_{mag} = \alpha - \alpha_{phon}$ using the data for YCu_2. We estimated the upper limit for the phonon contribution from the Debye model after performing the corresponding mass corrections [28] and using the maximum possible value for $\Gamma\chi$ (doted line in Fig. 9). The magnetic contribution is shown in Fig. 10. A narrow and strong peak appears at the quadrupolar transition, indicating a large reduction in the cell volume when the quadrupolar moments become ordered. In the paramagnetic region, we observed a broad hump centred around 50 K, which is likely to be due to crystal field effects. We analyzed the hump using the phenomenological model given in [29]; according to this model the contribution of the CEF splitting to $\alpha(\alpha_{CEF})$ follows the equation:

$$\alpha_{CEF} = \frac{\chi}{3V_m k_B T^2}\left[\langle E_i^2 \Gamma_i\rangle - \langle E_i\rangle\langle e_i \Gamma_i\rangle\right]$$

where k_B is the Boltzmann constant, Γ_i is the Grüneisen

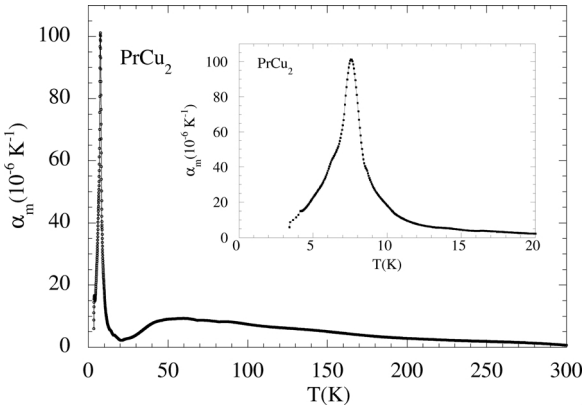

Fig. 10. Magnetic contribution to the linear thermal expansion coefficient of $PrCu_2$. The insert shows the low temperature part.

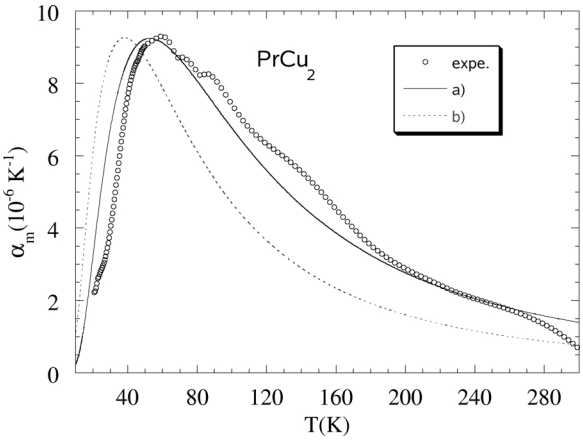

Fig. 11. Comparison between the magnetic contribution to the thermal expansion above the quadrupolar transition and the calculated data obtained from CEF splitting of refs. [12] (a) and [13] (b), see text.

parameter associated with the E_i level and the symbol $\langle\,\rangle$ represents thermal averages over the Bolztmann distribution. If we do not know the E_i and the Γ_i values, it may be meaningless to fit the experimental data using the equation because of the large number of fitting parameters in the equation. However, if we use the E_i values given in the literature and assume that all the Grüneisen parameters have the same value Γ [30], then we have only one parameter left as a fitting parameter which is $\chi\Gamma = \partial \ln E/\partial P$.

In Fig. 11 are shown the theoretical α_{CEF} curves for the CEF levels given in refs. [11] (curve a) and [12] (curve b) obtained for $\chi\Gamma = 14.4\,\mathrm{Mbar}^{-1}$ in both cases. The best agreement is found for curve a, which fits quite well the experimental data. We also checked the CEF levels given in ref. [3], but in this case the theoretical curve shows a broad maximum centred at T = 160 K. If we assume that the compressibility of $PrCu_2$ is an average of the compressibility of the pure elements [31], *e. g.* $\chi = 1.55\,\mathrm{Mbar}^{-1}$, then we can obtain the value of the Grüneisen parameter $\Gamma = 9.5$, which is similar to that found for $CeNi_{0.8}Pt_{0.2}$ ($\Gamma = 10$) [32]. Using the above value of the compressibility and the parameter $\Gamma\chi$ previously obtained for the lattice, it is also possible to estimate the Grüneisen parameter associated with the phonons: $\Gamma_{phon} = 1.7$.

Conclusions

The substitution of Pr by 20 % La/Y does not modify the crystalline structure of pure $PrCu_2$ and only increases/decreases the cell volume in agreement with the different ionic radii. The quadrupolar transition does not disappear with doping, but shifts from T = 7.7 K to lower temperatures nearly in proportion to the Pr percentage. The small difference between the transition temperatures in $Pr_{0.8}La_{0.2}Cu_2$(T_Q = 4.9 K) and $Pr_{0.8}Y_{0.2}Cu_2$(T_Q = 5.4 K) could be due to the different Pr–Pr distances in both compounds. In this sense, the increase of the Pr–Pr distance in the La doped compound with respect to the Y doped one reduces the quadrupolar interactions between the Pr ions and thus decreases the temperature of the quadrupolar transition. In addition we have found that the quadrupolar transition in $PrCu_2$ is very robust against magnetic field and does not disappear up to 20 T. Regarding the metamagnetic transition observed at high magnetic fields in single crystalline compounds, we have not found any sign of it in our polycrystalline samples. The electrical resistivity and the thermal expansion provide clear evidence of crystal field excitations at high temperatures. For the resistivity, neither of the previously proposed CEF models can account quantitatively for the experimental data, however for the thermal expansion the model proposed in [12] fits our results reasonably well. These analyses, in which the separation of the phonon and magnetic contributions was necessary, have allowed us to obtain benchmark values for Debye temperatures and Gruneisen parameters.

Acknowledgements

I thank Dr. G. Chouteau and Dr. J. G. Park for their help in the high magnetic field measurements and Dr. S. Zochowski for the thermal expansion measurements with the capacitance cell. Work at the High Magnetic Field Laboratory was supported by the HCM programme of the EC. I have also benefited from discussions with Dr. M. Ellerby and Dr. J. G. Park. I specially acknowledge Prof. K. A. McEwen and his group at University College London, where the samples were prepared during my sabbatical stay, for their kind support and hospitality. Finally, the financial support from Spanish CICYT Grant MAT 2005-06806-C04-02 is acknowledged.

[1] P. Morin, D. Schmitt, in: *Ferromagnetic Materials*, Vol. 5 (Eds.: K. H. J. Buschow, E. P. Wohlfarth), Elsevier, New York, **1990**.

[2] H. C. Walker, K. A. McEwen, D. F. McMorrow, S. B. Wilkins, F. Wastin, E. Colineau, D. Fort, *Phys. Rev. Lett*. **2006**, *97*, 137203.

[3] P. Ahmet, M. Abliz, R. Settai, K. Sugiyama, Y. Onuki, T. Takeuchi, K. Kindo, S. Takayanagi, *J. Phys. Soc. Jpn*. **1996**, *65*, 1077 – 1082.
[4] T. Takeuchi, P. Ahmet, M. Abliz, R. Settai, Y. Onuki, *J. Phys. Soc. Jpn*. **1996**, *65*, 1404 – 1408.
[5] J. K. Kjems, H. R. Ott, S. M. Shapiro, K. Andrés, *J. Phys*. **1978**, *C6*, 1010 – 1012.
[6] K. Andrés, E. Bucher, J. P. Maita, S. Cooper, *Phys. Rev. Lett*. **1972**, *28*, 1652 – 1655.
[7] R. M. Nicklow, R. M. Moon, *J. Appl. Phys*. **1985**, *57*, 3784 – 3788.
[8] S. Kawarazaki, J. Arthur, *J. Phys. Soc. Jpn*. **1988**, *57*, 1077 – 1086.
[9] A. Schenck, F. N. Gygax, Y. Onuki, *Phys. Rev. B* **2003**, *68*, 104422.
[10] M. Wum, N. E. Phillips, *Physics Letters* **1974**, *50A*, 195 – 196.
[11] J. K. Kjems, in: *Electron Phonon Interaction and Phase Transition* (Ed.: T. Riste), Plenum Press, New York, **1977**, p. 302.
[12] S. Zajac, *Acta Phys. Slov*. **1981**, *2*, 185 – 186.
[13] M. Andrecut, I. Pop, I. Burda, *Mater. Lett*. **1993**, *16*, 206 – 209.
[14] R. Settai, M. Abliz, P. Ahmet, K. Motoki, N. Kimura, H. Ikezawa, T. Ebihara, H. Sugawara, K. Sugiyama, Y. Onuki, *J. Phys. Soc. Jpn*. **1995**, *64*, 383 – 386.
[15] K. Sugiyama, P. Ahmet, M. Abliz, H. Azuma, T. Takeuchi, K. Kindo, H. Sugawara, K. Motoki, H. Ikezawa, T. Ebihara, R. Settai, Y. Onuki, *Physica B* **1995**, *211*, 145 – 147.
[16] Y. Hashimoto, K. Kindo, T. Takeuchi, K. Senda, M. Date, A. Yamagishi, *Phys. Rev. Lett*. **1994**, *72*, 1922 – 1924.
[17] J. Rodríguez Fernández, J. C. Gómez Sal, *J. Phys. D: Appl. Phys*. **1988**, *21*, 1165 – 1170.
[18] J. Rodríguez-Carvajal, FULLPROF, A. Program for Rietveld Refinement and Pattern Matching Analysis, *Physica B*, **1993**, *192*, 55 – 69.
[19] J. Rodríguez Fernández, J. Sánchez Marcos, J. I. Espeso, J. C. Gómez Sal, K. A. McEwen, *J. Alloys Compd*. **2001**, *323 – 324*, 384 – 388.
[20] J. C. Gómez Sal, J. Rodríguez Fernández, R. J. López Sánchez, *Solid State Commun*. **1986**, *59*, 771 – 776.
[21] J. A. Blanco, J. C. Gómez Sal, J. Rodríguez Fernández, D. Gignoux, D. Schmitt, J. Rodríguez-Carvajal, *J. Phys.: Condens. Matter*. **1992**, *4*, 8233 – 8244.
[22] J. A. Blanco, D. Gignoux J. C. Gomez Sal, J. Rodríguez Fernández, D. Schmitt, *J. Magn. Magn. Mater*. **1992**, *104 – 107*, 1285 – 1286.
[23] V. U. S. Rao, W. E. Wallace, *Phys. Rev. B* **1970**, *2*, 4613 – 4616.
[24] J. Rodríguez Fernández, K. A. McEwen, S. W. Zochowski, *J. Magn. Magn. Mater*. **1996**, *161*, 220 – 230.
[25] B. Lüthi, M. E. Muller, K. Andres, E. Bucher, J. P. Maita, *Phys. Rev. B* **1973**, *8*, 2639 – 2648.
[26] G. T. Meaden, *Electrical resistance of metals*, Plenum Press, **1965**.
[27] J. I. Espeso, J. Rodríguez Fernández, J. C. Gómez Sal, J. A. Blanco, *IEEE Transactions on Magnetics* **1994**, *30*, 1009 – 1011.
[28] J. A. Blanco, M. de Podesta, J. I. Espeso, J. C. Gómez Sal, C. Lester, K. A. McEwen, N. Patrikios, J. Rodríguez Fernández, *Phys. Rev. B* **1994**, *49*, 15126 – 15132.
[29] T. H. K. Barron, J. G. Collins, G. K. White, *Adv. Phys*. **1980**, *29*, 609 – 730.
[30] J. I. Espeso, J. Rodríguez Fernández, J. A. Blanco, J. C. Gómez Sal, *Solid State Commun*. **1993**, *87*, 735 – 739.
[31] B. Chevalier, J. Sanchez Marcos, J. Rodríguez Fernández, M. Pasturel, F. Weill, *Phys. Rev. B* **2005**, *71*, 214437.
[32] J. Rodriguez Fernández, J. I. Espeso, J. A. Blanco, J. C. Gómez Sal, *Physica B* **1993**, *186 – 188*, 618 – 620.